

Detecting Qubit-coupling Faults in Ion-trap Quantum Computers

Andrii O. Maksymov

Jason Nguyen

Vandiver Chaplin

IonQ

College Park, Maryland, USA

Yunseong Nam

IonQ

College Park, Maryland, USA

Department of Physics, University of
Maryland

College Park, Maryland, USA

Igor L. Markov

IonQ

College Park, Maryland, USA

ABSTRACT

Ion-trap quantum computers offer a large number of possible qubit couplings, each of which requires individual calibration and can be misconfigured. We develop a strategy that diagnoses individual miscalibrated couplings using only log-many tests. This strategy is validated on a commercial ion-trap quantum computer, where we illustrate the process of debugging faulty quantum gates. Our methodology provides a scalable pathway towards fault detections on a larger scale ion-trap quantum computers, confirmed by simulations up to 32 qubits.

KEYWORDS

quantum computers, ion traps, calibration, faults, testing

1 INTRODUCTION

Quantum computation [30] promises to extend the capabilities of conventional computers in science applications [16, 18, 27], for hard optimization problems [9, 32], and for sensitive cryptography tasks [28, 37]. Small and intermediate-scale quantum computers based on supercold superconductors [15, 33] and on moderately cooled trapped ions [14, 41] have now been offered commercially via cloud access for five years, as HW accelerators. Improving their operational uptime requires system stability, effective maintenance operations, and fast diagnosis of common problems.

Compared to conventional VLSI circuit test, several essential differences can be seen in testing and debugging of quantum circuits. In particular, testing and calibration are performed frequently between production runs as part of routine maintenance. The following executive summary is applicable to most qubit technologies except for photonic qubits.

- Each qubit represents a unit of storage, and gates are applied to qubits with sequential semantics.
- Qubits are short-lived and must be re-initialized often.
- The initial state of each qubit is zero; while an arbitrary bit-string can be configured via inverters, creating an arbitrary quantum state for test purposes is impractical.
- Quantum states are observed via stochastic destructive measurement, giving only partial information about the states.
- Individual gates are ephemeral and invoked via control signals with flexibility to execute different gates and circuits.
- Quantum noise, qubit decoherence, and typical faults are very different from any phenomena observed in CMOS circuits. In particular, stuck-at faults run against the unitary evolution implemented by quantum circuits.

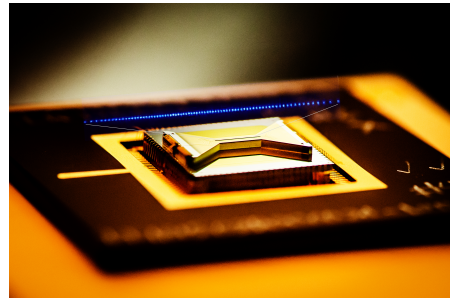


Figure 1: A packaged ion trap (HOA2) on a 15mm chip developed at Sandia National Lab. A chain of $^{171}\text{Yb}^+$ ions spaced at $4\mu\text{m}$ is illustrated by overlaying a different, magnified false-color image (blue dots) along the trapping axis. A qubit ion excited by a laser fluoresces (at UV wavelengths) or not depending on the quantum state, which helps perform quantum measurement. Image credit: Kai Hudek at IonQ.

Compared to scanning many test inputs into a static CMOS chip and observing intermediate values, quantum computers are tested by feeding an all-zeros initial state to a variety of test circuits which are reconfigured in an FPGA-like fashion. Observed measurement results are nondeterministic, which requires repeating everything many times to collect sufficient statistics.

Whereas conventional computing is dominated by CMOS-based ICs, many promising quantum computing hardware platforms are currently in active R&D. Quantum bits (qubits) can be carried by (i) photons, (ii) ions suspended in vacuum, and even (iii) quantized currents in superconducting loops. This work focuses on commercial¹ quantum architectures where trapped ions are suspended in a vacuum by electric fields [31]. The ions are laser-cooled to form a crystalline structure, typically a linear chain in the so-called linear Paul trap [5] (Figures 1 and 3). This architecture limits sources of noise that may disturb quantum information, and leading implementations report a stability window (coherence time) of 10^{11} sec for amplitudes (T_1 time) and 90 min for phases (T_2 time) [40].²

¹Here *commercial* means “supporting paying customers.”

²Long T_1 and T_2 coherence times are crucial metrics for reliable quantum computation. Short coherence times limit the depth of quantum computations before the information is lost to decoherence. Quantum error correction (QEC), if applied before a decoherence event occurs, can extend the computation time, but today’s physical systems lack sufficient resources to implement effective QEC.

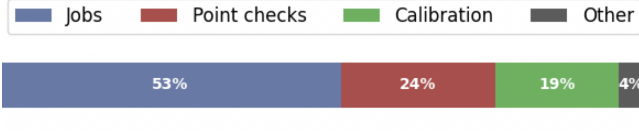


Figure 2: A typical lifecycle of a contemporary commercial ion-trap QC. Roughly 53% of time is spent to run QC jobs. The remaining 47% is used to test and calibrate various device aspects, including qubit couplings.

Among the advantages of ion-trap quantum computers are the perfect replicability of qubits within a device, all-pair qubit connectivity, as well as clean and relatively fast readout [24]. Unlike many competing architectures, where qubits need to be manufactured, ion qubits are naturally available, as atoms, and are identical every time. Operations on atoms such as creating ions by stripping electrons from neutral atoms, processing quantum information encoded in the internal states of the ion qubits, and reading out the states, are performed with laser beams [41], a mature technology that has been around for decades. Spectroscopic qubit readout is fast and clean and one can faithfully determine the measured state of the qubit [13]. Unlike with superconducting qubits, any pair of ion qubits can be directly coupled with no overhead to shuttle the quantum information around. While ion-trap QCs have much slower gates, their advantage in qubit lifetimes and all-pairs connectivity compensates for this when running quantum algorithms, as shown in a detailed comparison of two leading quantum architectures [21].

With the power to couple arbitrary pairs of qubits, comes the responsibility to ensure that qubit couplings are properly calibrated and can perform accurate gate operations [22]. Therefore, the lifecycle³ of an ion-trap QC interchanges operational periods and rounds of recalibration. Figure 2 outlines the lifecycle of a commercial ion-trap QC. Testing and calibration take almost half of the time, with significant overhead in identifying miscalibrated qubit couplings. For each new check, different control signals must be uploaded and measurements must be repeated to collect statistics. In more mature QC systems with improved coupling quality, more subtle faults will need to be detected, making fault detection more difficult. Testing $\binom{N}{2}$ qubit couplings, now already at a quarter of the ion-trap QC lifecycle, is going to consume a larger fraction of time as QC systems scale up. Hence, the need to optimize fault detection.

In this paper, we aim to improve the ion-trap lifecycle and speed up recalibration by efficiently diagnosing faulty qubit couplings. Brute-force diagnosis that checks qubit couplings one at a time scales poorly and is typically limited to testing a small subset of couplings and recalibrating them as necessary. Testing multiple couplings at a time scales better, can identify faulty couplings, and offers two avenues for improvements: (1) faster recalibration of faulty couplings, (2) delayed calibration by mapping quantum circuits around detected faulty couplings. To this end, our key contributions are

- A three-axis classification of quantum faults in ion-trap QCs.

³Here, *lifecycle* refers to the duration over which the ion chain can be used as a quantum computer. When the chain is lost, a new chain must be loaded and settled. This time is excluded from the lifecycle.

- Fault modelling for most common faults in the commercial architecture we explore.
- Testing protocols that quickly identify faulty qubit couplings among $\sim N^2$ possibilities using only $O(\log N)$ tests, always faster than binary-search strategies.
- A three-way validation of the protocols — via proofs, on a commercial QC, and using simulation to illustrate scaling.

In the remaining part of the paper, Section 2 reviews abstract quantum circuits and how they are implemented on ion-trap architectures. Section 3 offers a classification of faults in ion-trap quantum computers and focuses on modelling the dominant fault types in near-term implementations. Section 4 formalizes the problem we solve in Section 5, where we propose fault-testing protocols for diagnosing the faulty qubit couplings. In addition to proofs of correctness, we then offer validation based on experiments with a commercial ion-trap QC (Section 6) and simulation (Section 7).

2 BACKGROUND

The promise of quantum computing is not in higher device density or more computational steps per second, but rather in a new model of computation that requires fewer computational steps to solve some tasks [30]. To this end, we review quantum circuits and outline how they are implemented on ion-trap quantum computers.

2.1 Abstract quantum circuits

Quantum information is represented in states of quantum systems, such as collections of interacting trapped ions [41] or other physical systems. Instead of 0-1 bits, quantum bits (qubits) are used. In isolation, each qubit represent a two-dimensional complex-valued vector (α, β) with $|\alpha|^2 + |\beta|^2 = 1$. The *computational basis* states $(1, 0)$ and $(0, 1)$ are shortened to $|0\rangle$ and $|1\rangle$, respectively, and a general one-qubit state is written as $|\psi\rangle = \alpha|0\rangle + \beta|1\rangle$ [30]. Measuring $|\psi\rangle$ w.r.t. the basis states changes it to either $|0\rangle$ or $|1\rangle$ with probabilities $|\alpha|^2$ and $|\beta|^2$, respectively. Physical details of ion-trap qubits are discussed in Section 2.2, but the formalism holds for many technologies, such as superconducting and photonic qubits.

Quantum and conventional information differ in many ways, e.g., note a continuum of possible qubit configurations from which conventional information is extracted by destructive measurements. Another key distinction is in how subsystems can interact with each other. Conventional bit configurations are concatenated as strings, and the composite space grows as 2^n for n bits. Quantum bits can also be concatenated, e.g., $|0\rangle|1\rangle$ can be rewritten as $|01\rangle$, but for qubit states in superpositions we have:

$$\left(\frac{|0\rangle + |1\rangle}{\sqrt{2}}\right) \otimes \left(\frac{|0\rangle + |1\rangle}{\sqrt{2}}\right) = \frac{1}{2}(|00\rangle + |01\rangle + |10\rangle + |11\rangle).$$

The resulting superposition is clearly *separable*, but removing one term, say, $|01\rangle$ revokes separability and creates an *entangled state*. Quantum computing cannot outperform conventional computing without entanglement because separable computations can be simulated on conventional computers efficiently.

Quantum circuits typically start at a fixed state, such as $|000\dots 0\rangle$ (sometimes shortened to just $|0\rangle$) and apply a sequence of allowed operations, which end with qubit measurements [24]. Before measurement, an ideal quantum computer preserves the state-vector

norm and only applies *unitary* operators U .⁴ Most technologies today directly support only operators that modify one or two qubits at a time. Such operators are described by templates called *quantum gates* which can be instantiated on any qubit or pairs of qubits. Single-qubit gates include inverters (X gates) that swap $|0\rangle$ and $|1\rangle$, Z gates that negate $|1\rangle$, Phase gates that replace $|1\rangle$ with $i|1\rangle$, and Hadamard gates that create superpositions of basis states $\sigma_x = X = \begin{bmatrix} 0 & 1 \\ 1 & 0 \end{bmatrix}$ $\sigma_y = Y = \begin{bmatrix} 0 & -i \\ i & 0 \end{bmatrix}$ $\sigma_z = Z = \begin{bmatrix} 1 & 0 \\ 0 & -1 \end{bmatrix}$ $P = \begin{bmatrix} 1 & 0 \\ 0 & i \end{bmatrix}$ $H = \frac{1}{\sqrt{2}} \begin{bmatrix} 1 & 1 \\ 1 & -1 \end{bmatrix}$. Unlike these discrete gates, three Pauli-axis rotations $R_x(\theta)$, $R_y(\theta)$, and $R_z(\theta)$ perform angle- θ rotations.

$$R_x(\theta) = \exp(-i\theta X/2) = \begin{bmatrix} \cos \frac{\theta}{2} & -i \sin \frac{\theta}{2} \\ -i \sin \frac{\theta}{2} & \cos \frac{\theta}{2} \end{bmatrix}$$

$$R_y(\theta) = \exp(-i\theta Y/2) = \begin{bmatrix} \cos \frac{\theta}{2} & -\sin \frac{\theta}{2} \\ \sin \frac{\theta}{2} & \cos \frac{\theta}{2} \end{bmatrix}$$

$$R_z(\theta) = \exp(-i\theta Z/2) = \begin{bmatrix} \exp(-i\frac{\theta}{2}) & 0 \\ 0 & \exp(i\frac{\theta}{2}) \end{bmatrix}$$

Any single-qubit unitary operator can be written as a product of three axial rotations, whereas the gates X, Y, Z, P can be seen as special cases of these rotations. However, single-qubit gates alone cannot create entanglement. Common entangling two-qubit gates are Controlled-NOT (CNOT) and Controlled-Z (CZ) [30]. They do not modify the *control* qubit, but apply either X or Z on the *target* bit subject to $|1\rangle$ on the control bit. For example, CNOT maps $\frac{|0\rangle+|1\rangle}{\sqrt{2}} \otimes |1\rangle$ to $\frac{|01\rangle+|10\rangle}{\sqrt{2}}$. Given that $X = H Z H$, we also note that $\text{CNOT} = (I \otimes H)\text{CZ}(I \otimes H)$. Therefore, direct hardware support is often provided for only one of CNOT and CZ.

2.2 Ion-trap quantum computers

In a $^{171}\text{Yb}^+$ ion, computational basis states $|0\rangle$ and $|1\rangle$ are encoded in the energy levels $|F = 0, m_F = 0\rangle$ and $|F = 1, m_F = 0\rangle$ of the $^2S_{1/2}$ ground state, respectively.

Initialization and readout of typical ion qubits are performed using laser beams. Prior to any quantum computational operations, the ion chain is trapped and laser-cooled to the motional ground state using an efficient cooling method [4]. As a result, a chain of room-temperature ions can be brought down to μK temperatures in tens of milliseconds. *Optical pumping* then initializes a qubit to the $|0\rangle$ state with high accuracy in $\sim 20\mu\text{s}$. During measurement, laser light resonant with the $^2S_{1/2} |F = 1\rangle$ to $^2P_{1/2}$ transition induces fluorescence, allowing for each ion to be imaged by individual photodetectors when illuminated, determined to then be in the $|1\rangle$ or $|0\rangle$ state, which typically take $\sim 100\mu\text{s}$. Fast photo-detectors have been demonstrated with crosstalk between adjacent ions $< 10^{-4}$ [6].

Quantum gates, applied to evolve the state of quantum computers, are implemented in an ion-trap quantum computer by illuminating the ions by another set of laser beams. Modulating the beams helps implement single-qubit gates, where the illuminated ion's state is gradually rotated on the *Bloch sphere* about the desired Pauli axis.

⁴Unitary operators are those satisfying $UU^* = I$. Equivalently, unitary operators preserve norms and dot products.

More complicated dynamics and modulation [2, 11, 19, 43] are used to realize the canonical Mølmer-Sørensen (MS) two-qubit gate [38, 39], which implements an $XX(\theta) = \exp(-i\theta\sigma_x \otimes \sigma_x/2)$. This gate uses vibrational modes of the ion chain as the medium of information exchange, akin to a memory bus. A CNOT gate can be expressed via an MS gate and single-qubit gates as follows [23]: $\text{CNOT} = (R_y(\pi/2) \otimes I)(R_x(-\pi/2) \otimes R_x(\pi/2))XX(\pi/2)(R_y(-\pi/2) \otimes I)$. Clearly, the MS gate and single-qubit gates provide universality, i.e., can implement an arbitrary quantum operator [36]. Typical gate *fidelity* (Section 3) of an MS gate is $\sim 96.5\%$, whereas for a single-qubit gate it is $\sim 99.5\%$. The best reported fidelities are orders of magnitude better [1, 10, 13], suggesting room for near-term improvement.

All-pairs qubit connectivity is common for ion-trap architectures and allows any two qubits to be entangled directly. This is natural since each and every ion participates in a vibration bus. All-pairs qubit connectivity provides a decisive advantage in harnessing the computational power of an ion-trap QC [12], and often the feasibility of a given computation on a given QC [21]. Applying fast gates to a remote qubit pair requires substantially more power in the driving signals than for a nearby pair [3]. Therefore, just like in VLSI layouts, shorter connections are preferred.

Control accuracy required to perform high-fidelity ion-trap quantum computation [20] is assessed in terms of the trapping field and the beams that illuminate the qubits. The former ensures proper geometric placement of trapped ions and with suitable vibrational behaviors. The latter ensure the alignment of optical signals with qubits. Control loss occurs in several ways. Stray fields in the ion trap are a common problem, one of leading causes is incidental charging of trap electrode surfaces. Even very small stray fields interfere with the trapping electric field and slowly displace ions from their ideal locations, indirectly degrading the quality of quantum gates. Understanding these mechanisms suggests restorative action. Since typical operation of an ion-trap quantum computer intentionally applies extra electric fields to the trap electrodes, we can use them to return ions to their optimal positions. This recalibration of ion positions can compensate for slowly-varying stray fields. Gate operations on ion qubits are performed using a pair of overlapping laser beams, requiring accurate control of beam geometry and power. Optomechanical stability is thus needed in order to avoid positional and power drifts. Additionally, the light used to illuminate the qubits results in significant light-induced static and dynamic frequency shifts of the qubit states. These *light shifts* are challenging to model [17].

Component recalibration is performed in two phases: measurement and correction. In one example, we gradually shift the beam position and monitor ion response. In addition to geometric calibration, ion-qubit gates are also routinely calibrated to compensate for any optical power drifts. Respective light shifts are measured and accounted for in the execution of control algorithms. Unfortunately, it is not practical to measure every relevant parameter, therefore recalibration is either repeated at regular intervals or triggered by a failing canary, i.e., a representative monitored value falling below an acceptable threshold. Lacking accurate up-to-the-minute information about physical drifts leads to significant recalibration efforts that are not entirely necessary.

Benchmarking a quantum computer assesses not only individual components but also their integration and the overall functional

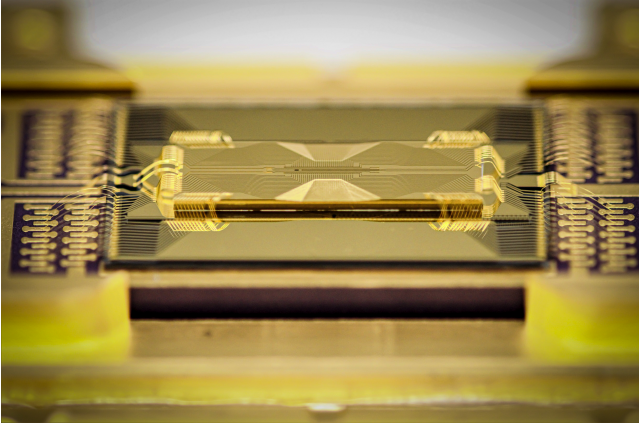


Figure 3: A 14mm long, high optical access, IonQ-designed trap packaged on an interposer. Ions are loaded by ionizing a neutral beam of Yb atoms introduced through a load slot in the left region of the trap. The ionized atoms are laser-cooled and then shuttled to the quantum zone in the center of the image. Image credit: Walker Steere at IonQ.

performance. A full characterization of a quantum process in an N -qubit system requires exponentially large computational resources in N . Thus, system errors are evaluated by simplified methods, such as randomized benchmarking (RB) [7]. RB essentially applies a random sequence of gates drawn from a restricted set of gates. Assuming the errors are non-systematic and Markovian, efficient estimation of the size of the errors associated with the gates in the set becomes possible. Multiple variations of RB are reported in the literature, such as cycle benchmarking (CB) [8], allow one to further and better characterize quantum gates and circuit elements with a more advanced and realistic model of errors.

3 FAULT CHARACTERIZATION & MODELS

To address the non-ideal operation of a quantum computer, we classify such behaviors by their determinism and unitary evolution properties. An ideal QC should be deterministic before quantum measurement but this is not always the case. For example, qubit decoherence on QCs with low T_1 and/or T_2 times can limit the depth of quantum computation. The evolution of properly isolated quantum states, as described by Schrödinger equation, is unitary unless affected by stray interactions. Table 1 discusses four types of quantum faults along these axes. A third axis in our classification accounts for the time scale. Slow noise may look deterministic during one QC run but not at a longer time scale.

A QC free of noise and errors produces the correct output state which then determines the probabilities of measurement outcomes. For example, if a two-qubit circuit results in a fully entangled state $\frac{1}{\sqrt{2}}(|00\rangle + |11\rangle)$ then there should be a 50% chance to measure the system in either $|00\rangle$ or $|11\rangle$ states while the probabilities to measure it in either $|01\rangle$ or $|10\rangle$ states should be zero. Errors present in real devices change the distribution of output probabilities [2, 3], contributing to imperfect gate fidelities.

Gate fidelity estimation. Formally, gate fidelity \mathcal{F} captures the similarity of an ideal unitary gate U and the actual quantum operation \tilde{U} performed, i.e., $\mathcal{F} := 1 - |U - \tilde{U}|$ for some operator norm $|\cdot|$. Popular choices include the Frobenius norm, as well as the diamond, spectral and other norms. In practice, estimating fidelity can be difficult because the matrix \tilde{U} is not easily available. Since the dominant failure modes of contemporary MS gates on ion-trap QCs are known, it is common to use approximate methods, which we illustrate next.

On an ion-trap QC, MS gates tend to have smaller gate fidelities than single-qubit gates. In the literature [2, 3], MS gate fidelities are typically approximated by first applying $XX(\pi/2)$ to $|00\rangle$ and measuring (i) the populations of $|01\rangle$ and $|10\rangle$ and (ii) the balance between the populations of $|00\rangle$ and $|11\rangle$. Note that in the absence of inaccuracies the generated state should be $\frac{1}{\sqrt{2}}(|00\rangle - i|11\rangle)$, so that the lack of $|01\rangle$ and $|10\rangle$ and the balance between $|00\rangle$ and $|11\rangle$ are indicative of perfect gate fidelity.

As a more detailed example, consider evaluating the MS-gate fidelity in the case where $XX(\pi/2)$ induces a perfect balance between $|00\rangle$ and $|11\rangle$. When the gate is applied to, say, ions i and j , the average fidelity (over arbitrary two-qubit input states) may be computed as [2, 3, 42]

$$\mathcal{F} = 1 - \frac{4}{5} \sum_{p=1}^n [\eta_{p,i}^2 + \eta_{p,j}^2] |\alpha_p|^2, \quad (1)$$

where $\eta_{p,i}$ is the so-called Lamb-Dicke parameter that denotes the coupling strength between the p th vibrational (normal) mode and the i th ion and α_p is the error incurred in the decoupling of the mode p from any one of the ions at the end of an MS gate, required for a perfect MS-gate implementation, that corresponds to the amount of quantum information unintentionally left behind in a memory bus.⁵ In short, the *infidelity* $1 - \mathcal{F}$ of an MS gate on an ion-trap QC is characterized by the residual, incorrect coupling between the ions i and j that the MS gate is applied to and the vibrational modes. The infidelity here can be directly measured as the sum of populations of $|01\rangle$ and $|10\rangle$.

Returning to a more realistic case with an imbalance between $|00\rangle$ and $|11\rangle$, the following expression is often used to compute the gate fidelity [11]:

$$\mathcal{F} = \frac{P_{|00\rangle}^* + P_{|11\rangle}^* + \Pi_{\text{contrast}}}{2}. \quad (2)$$

The two fidelity-determining circuits are $XX(\pi/2)$ and $(R_\phi(\pi/2) \otimes R_\phi(\pi/2))XX(\pi/2)$, where $R_\phi(\theta) = \exp(-i\theta(\cos(\phi)X + \sin(\phi)Y)/2)$. The initial state for both circuits is $|00\rangle$. Ideally, for the first circuit, as discussed above, we expect $P_{|00\rangle} + P_{|11\rangle} = 1$, where $P_{|ab\rangle}$ are the populations of the states $|ab\rangle$. We use P^* to denote the measured populations from this first circuit. For the second circuit, as a function of ϕ , we ideally expect $P_{|00\rangle} + P_{|11\rangle} - P_{|01\rangle} - P_{|10\rangle} = \sin(2\phi)$. If there is an imbalance between $|00\rangle$ and $|11\rangle$ that is induced due to implementing $XX(\pi/2 + \epsilon)$, however, instead of $\sin(2\phi)$, one obtains $\cos(\epsilon) \sin(2\phi)$. In practice $\Pi_{\text{contrast}} \sin(2\phi)$ is observed,

⁵For completeness: $\alpha_p := \int_0^\tau g(t) e^{i\omega_p t} dt$, where τ is the MS gate duration, $g(t)$ is the control pulse illuminating the ions, and ω_p is the angular frequency of mode p . See [2] for details.

	UNITARY	NON-UNITARY
DETERMINISTIC	Inexact calibration of beam intensity, e.g. due to light shift miscalibration, beam misalignment or wrong gain applied to the illuminating beams. Usually static in time.	Non-unitary violations of physical models: unintended bit flips induced by signals that correspond to vibrational bus excitation, sidebands or anharmonicity.
STOCHASTIC	Random parameter fluctuations due to heating, control signal noise in amplitude and frequency.	Double ionization event, loss of order, chain loss, etc.

Table 1: Types of quantum faults with respect to determinism and unitary evolution. A third axis accounts for the time scale.

$\Pi_{\text{contrast}} \leq \cos(\epsilon)$, since further contrast can be lost due to the information leakage to the bus. Experimentally, the value of Π_{contrast} is estimated via the best fit of ion-trap QC data.

The quality of these approximate methods can be tested directly by comparing theoretical predictions to experimental results. Results reported in the literature [2, 3, 42] show that the experimental results are in excellent agreement with the theoretical prediction. The agreement indicates the failure modes of MS gates on today’s ion-trap QCs are well understood, justifying our focus on the specific error models we discuss next.

Dominant faults and fault models. Experimental data [41] for leading ion-trap QCs suggest that, at this stage of development, unitary faults are most common and most impactful. Excellent isolation of trapped ions from non-unitary noise plays a big role here. In ion-trap QCs (and some superconductor QCs), coherence times T_1 and T_2 are orders of magnitude longer than the time needed to run a circuit [40], while state preparation and measurement errors (SPAM) are $<1\%$ and can be addressed in post-processing due to their stability [1, 34, 35]. On the other hand, the impact of unitary faults accumulates exponentially with the number of gates and modifies the final quantum state. When native gates are specified by their rotational axis and angle, most unitary errors impact the phase and/or the amplitude of a particular gate. Hence, our general fault models for single- and two-qubit unitary gate errors presented in Figure 5. Other unitary errors such as spillover (cross-talk) can be simulated by additional gates applied on *spectator* qubits. The residual coupling of the chain to the motional modes can also be simulated by additional random single-qubit rotations. Fault models in Figure 5 explain how faults accumulate under gate repetition: deterministic faults add up until a certain point (based on how unitary rotation matrices multiply).

Empirical validation of fault models: simulation vs physical observations. Phase and amplitude errors can be non-deterministic (due to noise and drifts) and deterministic (due to miscalibrations and alignment errors). Due to the high dimensionality of the quantum state space, non-deterministic errors accumulate at a significant rate, but slower than correlated deterministic errors [29]. We illustrate this in Figure 4 by simulation and by a direct experiment on an ion trap. Shown are infidelities of a sequence of MS gates concatenated in phase vs. in anti-phase for two ion pairs of an 11-ion chain. It can be noticed that gate fidelities differ between the two ion pairs due to the difference in noise and calibration errors. Our simulation models phase noise and residual coupling to the motional modes. As seen in Figure 4, our simulator and our fault models show reasonable agreement with experimental data. The dominance of deterministic unitary errors (systematic amplitude errors, etc.) gives us hope to find them with tests and eliminate them with recalibration. Multi-gate sequences can mitigate such

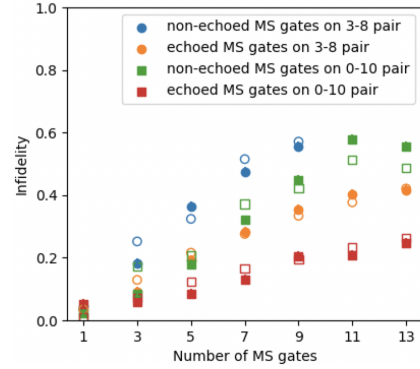


Figure 4: Measured (solid markers) and simulated (empty markers) infidelities of concatenated non-echoed and echoed MS gate sequences for {3, 8} (circles) and {0, 10} (squares) qubit pairs. Each circuit was measured in 1000 shots.

errors [2, 12, 25, 26], but they often are unsuccessful in the presence of other error sources.

4 QC TESTING: PROBLEM FORMULATION

Thanks to all-pairs qubit connectivity, $\binom{N}{2}$ different MS gates can be implemented on an N -qubit ion-trap QC. We consider the case where a small subset of qubit couplings are faulty and require calibration — other couplings maintain their earlier calibration. Based on the characterized faults that dominate today’s ion-trap QCs, we seek a testing strategy to find the faults quickly.

A typical ion-trap QC runs 1- and 2-qubit gates much faster than it can re-initialize qubits (using laser cooling, etc). Therefore, the runtime of a test with multiple MS gates is dominated by qubit initialization and readout, and we minimize the number of tests. For example, we can run a test circuit with one MS gate per coupling, excluding one particular qubit pair. If this test produces expected results, it would implicate the excluded qubit pair. More efficient strategies use *binary search* where each test narrows down the set of suspected couplings by a factor of two. Such strategies can succeed with arbitrary balanced partitions of couplings, requiring $\log_2 \binom{N}{2} \approx 2 \log_2 N - 1$ tests to identify a single faulty coupling (the worst case is only one test worse than the average case). As seen in Section 3 and Figure 5, quantum gates may be “slightly faulty”, and very small inaccuracies can be neglected. To make sure that above-threshold faults are detected, we repeat each gate several times in each test.

$$R(\theta, \phi) = \begin{bmatrix} \cos \frac{\theta}{2} & -ie^{-i\phi} \sin \frac{\theta}{2} \\ -ie^{i\phi} \sin \frac{\theta}{2} & \cos \frac{\theta}{2} \end{bmatrix} \quad M(\theta, \phi_1, \phi_2) = \begin{bmatrix} \cos \frac{\theta}{2} & 0 & 0 & -ie^{-i(\phi_1+\phi_2)} \sin \frac{\theta}{2} \\ 0 & \cos \frac{\theta}{2} & -ie^{-i(\phi_1-\phi_2)} \sin \frac{\theta}{2} & 0 \\ 0 & -ie^{i(\phi_1-\phi_2)} \sin \frac{\theta}{2} & \cos \frac{\theta}{2} & 0 \\ -ie^{i(\phi_1+\phi_2)} \sin \frac{\theta}{2} & 0 & 0 & \cos \frac{\theta}{2} \end{bmatrix}$$

Figure 5: A general fault model for one- and two-qubit unitary errors in ion-trap QCs.

Binary search is an *adaptive* testing strategy, where the results of prior tests determine the next test. However, such feedback and any required conventional computation to select the next test may be prohibitive without thorough hardware support because many *non-adaptive* tests can be performed before the next adaptive test is determined. For similar reasons, circuit-level test for conventional VLSI is largely non-adaptive. Therefore, one of our challenges is to develop efficient non-adaptive strategies, even if they require more tests than binary search.

Depending on how often we run the tests, multiple qubit couplings may need calibration. Binary search finds one fault among many, but also extends to multiple faults. In one such approach, all couplings with detected faults are removed from future tests, and binary search is repeated to find the remaining faults.⁶ As we show below, non-adaptive test strategies outperform binary search when multiple faults are present.

5 FAULT TESTING PROTOCOLS

In this section, we show that for multiple faults adaptive testing can be done more efficiently than with binary search, and non-adaptive tests can do most of the job. As is typical for textbook analysis of binary search, we simplify notation and analysis by first assuming that the number of qubits is a power of two $N = 2^n$. The more general analysis immediately follows by padding. For brevity of analysis, we assume that when a coupling is not faulty, all gates on this coupling enjoy perfect fidelity.

5.1 Prerequisite combinatorics

We index individual qubits with integers $0..2^n - 1$ and view these integers in binary. In this section, we investigate pairs of *distinct* integers $0..2^n - 1$ and whether they belong to certain large classes of integers. We separately study

- (1) *generic* pairs of integers with at least some bits in common,
- (2) pairs of integers that share bits in specified positions (or none) and have opposite bits in the remaining positions.

Define $2n$ classes labeled (i, b) , so that each class contains all integers whose i -th bit value is b , $i \in \{0, 1, \dots, n-1\}$ and $b \in \{0, 1\}$.

LEMMA 5.1. *Consider pairs of distinct non-complementary integers. Each pair is included in at least one class.*

PROOF SKETCH: to find such a class for a pair, it suffices to find a common bit shared by the two integers.

LEMMA 5.2. *For each $0 \leq i < n$, the classes $(i, 0)$ and $(i, 1)$ are complementary, and every pair of integers is in at most one of them.*

Since different n -bit integers can share at most $n-1$ bits,

⁶A different strategy would perform two tests at each step – testing a set of couplings and its complement. If both tests detect faults, the search procedure would branch two-way. But this appears less efficient when the number of faults is small but unknown.

LEMMA 5.3. *Every pair of distinct integers is in $\leq n-1$ classes.*

i	$b = 0$	$b = 1$
0	0, 2, 4, 6	1, 3, 5, 7
1	0, 1, 4, 5	2, 3, 6, 7
2	0, 1, 2, 3	4, 5, 6, 7

The integers $\{2, 7\}$ share bits at $i = 1$ and belong to the class $(1, 1)$. But $\{0, 7\}$, $\{1, 6\}$, $\{2, 5\}$, and $\{3, 4\}$ are bit-complementary and do not belong to any class.

We now turn to pairs of bit-complementary integers and define a set of $2n-2$ classes. Class labels will be $[i, =]$ and $[i, \neq]$ for $0 < i < n$. The classes contain integers with equal and unequal bits in positions $i-1$ and i , respectively.⁷ For such classes, we have

LEMMA 5.5. *For each $0 < i < n$, each bit-complementary pair of integers is included in one of $[i, =]$ and $[i, \neq]$.*

PROOF SKETCH: For two bit-complementary integers and any pair of bit indices $0 < i < n$, the $(i-1)$ -th and i -th bits are in the same relation ($=$ or \neq) for both integers.

i	$=$	\neq
1	0, 3, 4, 7	1, 2, 5, 6
2	0, 1, 6, 7	2, 3, 4, 5

The bit-complementary integers $\{2, 5\}$ have unequal bits at $i = 2$ and $i = 1$ (01 and 10, respectively), thus belong to the class $[2, \neq]$.

THEOREM 5.7. *No two bit-complementary pairs of integers belong to the same set of classes. The same holds for classes $[i, =]$ only.*

PROOF SKETCH: Given two different bit-complementary pairs, we can find an $0 < i < n$ such that the bits at positions $i-1$ and i of these pairs exhibit different ($=$ or \neq) relations. To make this argument constructive, we represent each pair by $n-1$ bits computed as \oplus (exclusive OR) of consecutive bits (same result for both integers), and then find different bits between the two pairs. For example, $(2, 5)$ would be represented by 11_b . Since the classes $[i, =]$ and $[i, \neq]$ are complementary, their membership information is redundant.

For a subset of $k < n$ bit indices and bit values, we now turn our attention to integers that have specified values at the k bit positions. We then consider pairs of such integers that are bit-complementary in the remaining bits. To adapt the construction of classes $[i, \cdot]$, we renumber the bits so that the k bits go first. Hence, $n-k-1 \leq n-1$ classes distinguish any two pairs, per Theorem 5.7.

5.2 A single-fault protocol

We now show how to identify a single faulty qubit coupling with $3n-1$ tests and a single round of adaptation after $2n$ tests. For each class, we perform one test that includes gates for each coupling between qubits in that class. Per Lemma 5.1, this tests all couplings

⁷Observe that $[i, =] = (\text{GrayCode}(i), 0)$ and $[i, \neq] = (\text{GrayCode}(i), 1)$.

except for those between qubits with binary-complementary indices. After performing these tests, we call the set of failing tests (i, b) a *syndrome*. Lemmata 5.1–5.3 yield the following:

COROLLARY 5.8. *Given a faulty coupling defined by a pair of distinct integers, a syndrome includes $\leq n - 1$ failing tests, with no repeating i values.*

LEMMA 5.9. *For a syndrome of length $0 < L < n$, 2^{n-L-1} pairs of integers result in the same syndrome.*

PROOF SKETCH: Fixing L bits out of n leaves 2^{n-L} integers. For each such integer, we complement all $n - L$ bits not fixed to obtain a pair with exactly L shared bits. Thus, there are $2^{n-L}/2$ pairs.

THEOREM 5.10. *A single faulty coupling can be found with $3n - 1$ tests and one round of adaptation after $2n$ tests.*

PROOF SKETCH: determining the syndrome takes $2n$ non-adaptive tests. For a syndrome of length L , Lemma 5.9 shows that 2^{n-L-1} pairs exhibit the same syndrome. To identify one pair out of 2^{n-L-1} , binary search needs $n - 1$ additional tests, but each test is adaptive. Instead, we use the $[i, =]$ classes defined earlier, adapted to $k = n - L$ bits not specified by the syndrome.

EXAMPLE 5.11. *For $n = 3$, the observed syndrome in the first round is $(0, 0) = \{0, 2, 4, 6\}$ and $(1, 1) = \{2, 3, 6, 7\}$ (hence, $L = 2$). This specifies two bits $*10_b$ and leaves $2^{n-L-1} = 1$ possibility: $\{2, 6\}$. However, in case the observed syndrome is only $(0, 0)$ (hence, $L - 1$ and $**0_b$), we have two possibilities: $\{0, 6\}$ and $\{2, 4\}$. To tell them apart, we test for $\{0, 6\}$ that have two equal leading bits.*

COROLLARY 5.12. *The claim of Theorem 5.10 holds even if some qubit couplings are not used.*

PROOF SKETCH: We exclude unused couplings from the test sets defined in Sections 5.1 and 5.2. Faults on remaining couplings are still distinguished by the tests.

Now that we have defined the tests and proven that they can distinguish any two faulty couplings, we need an algorithm that finds the unique faulty coupling given test results. Fortunately, the number of couplings is small enough for us to evaluate test results for each and compare them to observations.

5.3 Diagnosing multiple faults

With multiple faults, the first round of the single-fault protocol produces the union of syndromes of individual faults. For multiple pairs, the claims of Lemmata 5.2 and 5.3 will often not hold and further steps of our single-fault protocol won't find even one pair. Here we note that test-driven calibration makes little sense after catastrophic effects that create numerous faults. Therefore, we assume a small number of faults and diagnose them.

The key principle is to *use lightweight tests to separate faults in time and magnitude before trying to diagnose them*, whereas diagnosed faults can be separated by qubit couplings.

Before discussing specific strategies, we remind the reader that the time overhead of running a circuit on an ion-trap QC is dominated by qubit initialization and readout rather than by gate count, whereas deciding which circuit to run based on the output of earlier circuits is much more costly than running a circuit.

Fault separation in time relies on frequent (e.g., every minute) runs of a canary circuit with gates at all relevant qubit couplings, to detect the emergence of faults. A canary failure triggers fault diagnosis before numerous faults complicate testing.

Fault separation by magnitude. As seen in Figure 5, faulty couplings may be off by different amounts. In practice, these amounts are often small initially but grow over time. To amplify small faults for detection, we repeat each gate several times⁸, and the number of repetitions is easy to control. An initial (canary) test is performed with every gate repeated many times. When it detects the presence of a fault, we find the smallest number of repetitions that still detects the fault. This can be done using a binary search on the number of repetitions or a non-adaptive search that checks R different repetition counts but is likely to be faster in practice. When a single fault is associated with this magnitude threshold, it can be detected by the single-fault protocol.

Fault separation by qubit couplings removes the couplings with diagnosed faults from further testing and helps finding faults with smaller magnitude. Per Corollary 5.12, the single-fault protocol works in this case, but we need to find the next smallest number of gate repetitions as explained above.

The cost of fault detection is dominated by adaptive rounds and is also (but less) sensitive to the number of qubit initializations and measurements, i.e., the number of circuit runs (including those with the same circuit). To this end, canary runs that provide *fault separation in time* can use delayed feedback, i.e., the next circuit run does not need to wait for canary feedback, but would be aborted in those rare cases when a fault is detected. *Fault separation in time* is performed by non-adaptive search (optimized using statistics of past fault magnitudes). A third round of adaptation is included in single-fault diagnosis. One additional round can verify that the identified fault is indeed faulty, after which we test for faults with a smaller magnitude. The overall procedure finishes when, after separating previously diagnosed faults, magnitude search finds no more faults (hence, another adaptation). The costs are summarized as follows:

0 faults	periodic canary test runs (negligible)
k faults	$4k + 1$ adaptations

The number of circuit runs is $ks(3n + R)$ where s is the number of "shots" per circuit needed to collect statistics, and R is the number of gate repetition configurations checked by non-adaptive search.

6 PHYSICAL VALIDATION

In this section, we validate the fault-detection strategy detailed in the previous section. For this, we use an ion-trap QC hosted at IonQ. As a first step, we use a test that is readily available in experimental settings, called the *single-output test*. We investigate the test on well-pronounced artificial unitary errors that we introduce to the ion-trap QC and compare empirical results to those obtained from a unitary-error simulator, capable of simulating the kinds of errors

⁸If the fault on a qubit coupling, upon repetition, becomes undetectable due to the fault's accidental cancellation or becoming identity, it may be detected by inserting qubit swaps. Example: Suppose a coupling $\{2, 6\}$ is faulty such that applying the faulty operation twice in a row, applied to supposedly amplify the fault, cancels the effect of the fault. By inserting a swap between, for instance, qubits 5 and 6, the fault-detection test would then become calling (i) a faulty coupling between $\{2, 6\}$, (ii) a qubit swap between $\{5, 6\}$, and (iii) a non-faulty coupling between $\{2, 5\}$, thereby avoiding the accidental cancellation.

that dominate today’s ion-trap QCs. Upon confirming the agreement between the two, we again compare experimental data to and simulation results, however this time without introducing artificial errors. This directly targets the "natural" errors of ion-trap QCs. The observed agreement validates our error models used in the simulator, our fault-detection strategy, and its viability in practice.

Ion-trap QC at IonQ. We use an 11-qubit ion-trap QC for experiments. Each qubit is a $^{171}\text{Yb}^+$ ion, where the computational basis $|0\rangle$ and $|1\rangle$ is encoded in the hyperfine transition with splitting of $\sim 12.6\text{GHz}$. As explained in Section 2.2, two-qubit gates are nominally calibrated to guarantee 96.5% fidelity and single-qubit gate are nominally calibrated to guarantee 99.5% fidelity. The qubits are roughly evenly spaced, with the inter-spacing of about $\sim 4\mu\text{m}$, resulting in $\sim 3\text{MHz}$ frequencies of the motional modes we use as the medium of communication between qubits. T_1 time is immeasurably long (tens of thousands of years) and T_2 time is around 600ms. We note that while this system is limited in its scale, the working principles and the observed fault modes are representative of future ion-trap systems. Given the long T_1 and T_2 times, with the latter having been demonstrated to be more than an hour in the state-of-the-art experiment, we continue to expect unitary errors will be dominant for the foreseeable future.

Single-output tests. A single test corresponds to a single quantum circuit with multiple two-qubit gates. Here we need a circuit sensitive to the errors of interest, so we use the single-output test that (ideally) returns the system to its initial state. The test passes if the resulting state matches the initial state. Our tests that target deterministic unitary errors, such as miscalibrations. For example, if a fully-entangling MS gate is applied four times in a row onto the same qubit pair, it does not change the initial state in the absence of errors, while it applies $\text{XX}(4\epsilon)$ gate if there is a miscalibration that results in error ϵ per MS gate application. This is the rationale for a four-MS-gate, single-output test. The deviation of the output population from the all-zero state, with the all-zero initial state, is then indicative of the miscalibrated gates. A similar single-output test can use only two MS gates per pair with the difference being that the output is no longer the initial, all-zero state but an inverted, all-one state.

Testing artificially introduced errors. Here, we show experimental results for physical 8-qubit testing with sets of two and four stacked MS gates, and compare them with the simulations. Specifically, in an ion-trap QC, we introduce artificial 47% and 22% under-rotations on $\{0, 4\}$ and $\{0, 7\}$ qubit pairs, respectively, by adjusting amplitude of the beams illuminated for the qubit pairs. Each circuit was executed (and the results were measured) 300 times.

Target-state fidelities, calculated from the returned measurement outcomes, are shown in Figure 6. The obtained results show an excellent agreement with the simulated fidelities. Faulty tests can be resolved from non-faulty ones when compared to thresholds at ~ 0.45 for the two-MS-gate tests and at ~ 0.25 for the four-MS-gate tests. Since the main error source is of a unitary kind, we use a unitary simulator. In particular, in the simulator, we include 10% random amplitude errors for all two-qubit gates, residual coupling to the motional modes that generates 1% odd population (see Sec. 2.2), and $1/f$ phase noise (see Fig. 5).

Testing a commercial ion-trap QC in operation. Figure 7 shows a counterpart to Figure 6, except, this time, we do not introduce

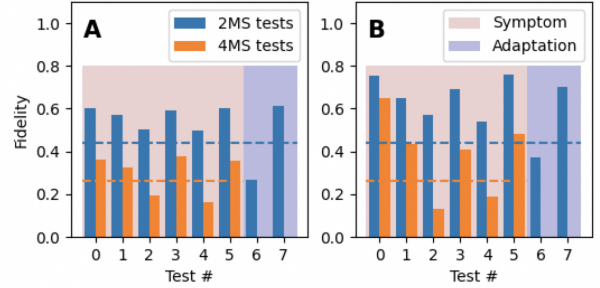


Figure 6: Measured fidelities of two-MS-gate tests (blue bins) and four-MS-gate tests (orange bins) with artificially-introduced 47% and 22% under-rotations on $\{0, 4\}$ and $\{0, 7\}$ qubit pairs, respectively, on 8 qubits. Panel A: Simulation. Panel B: Experiments. A positive test result can be determined by considering a fidelity threshold of 0.45 and 0.25 for the two- and four- MS-gate tests, respectively (dashed lines).

artificial miscalibrations. Instead, we calibrate all our two-qubit couplings, wait 15 minutes, then run our tests. This serves as a litmus test on the efficacy of our fault-detection strategy under a typical operation condition of a commercial ion-trap QC. Independently, we directly monitor the MS-gate quality, i.e., we track angles θ of $\text{XX}(\theta)$ gates, for cross comparisons. The largest miscalibration on $\{3, 4\}$ is diagnosed first with no positive test results.⁹ Subsequently, the other two faults on $\{2, 5\}$ and $\{5, 7\}$ are diagnosed by inserting fidelity thresholds at 0.38 (dashed orange line) and 0.46 (dashed red line), respectively.

7 VALIDATION VIA SIMULATION

To go beyond the scale limitations of the physical QC available to us, we now leverage simulation to investigate the scaling of our fault-detection strategy. Here we use the same simulator that we confirmed (in Section 6) to adequately model errors on our ion-trap QC (see Figure 7). Working with a simulator is particularly convenient, as we can create and explore in detail a variety of coupling fault configurations that (a) stress our fault-testing protocols and/or (b) represent realistic conditions in an ion-trap QC. For clarity of narrative, we suppress phase noise and residual couplings to the motional modes that we know to not affect the test outcomes in a significant way, leaving only 10% random amplitude errors. We simulate up to 32 qubits with this error model.

Figure 8 shows the fault contrast for larger numbers of qubits (8, 16, and 32), obtained from simulations of the two- and four-MS-gate tests. In the presence of 10% amplitude noise, the faulty qubit pair, in the single fault case, needs to be an outlier to be distinguished through tests. For the two-MS-gate tests, the minimum under-rotations for 8, 16 and 32 qubits are about 25%, 30%, and 35% respectively to be identified in 95% of the cases. Under the same

⁹This case results in no syndrome for the first six tests. The two tests we run after adaptation check for 01_b , i.e., we see if there is any fault between $\{0, 7\}$, $\{1, 6\}$ then $\{1, 6\}$, $\{2, 5\}$. Thus, the two additional tests also return nothing. Assuming a single-fault model, the faulty coupling $\{3, 4\}$ is identified. An additional test explicitly checking for $\{3, 4\}$ can be run to rule out the zero-fault case.

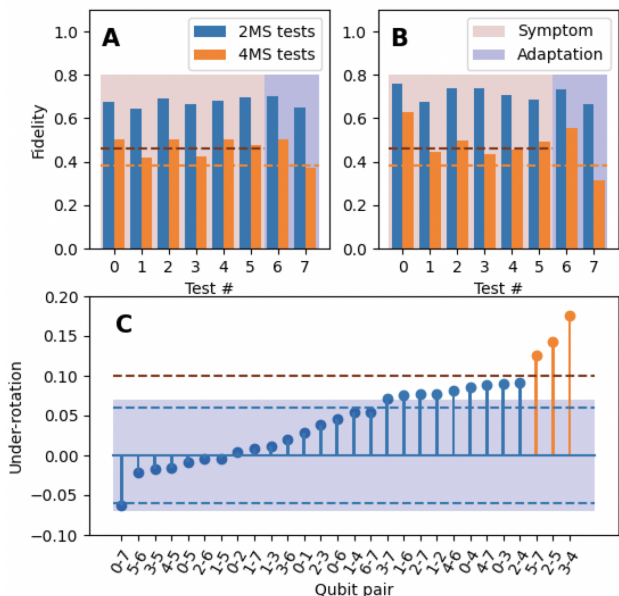


Figure 7: Measured fidelities of two-MS-gate tests (blue bins) and four-MS-gate tests (orange bins) with naturally occurred miscalibrations during a 15 min idling period. Panel A: Simulation. Panel B: Experiments. Positive test results for under-rotations of $\sim 15\%$ are determined by considering fidelity thresholds of 0.38 and 0.46 on four-MS-gate tests. Panel C shows the snapshot of the MS-gate quality at the 15th min. The blue area marks the region of under/over-rotations within 6%. The 10% under-rotation threshold is marked with a red dashed line.

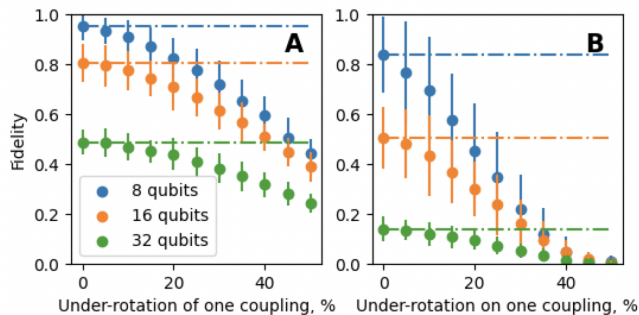


Figure 8: Simulated fidelities of two-MS-gate tests (panel A) and four-MS-gate tests (panel B) as a function of under-rotation on one qubit pair in the presence of 10% average calibration error for 8, 16 and 32 qubits. Dashed lines extend the average fidelity absent calibration outliers.

conditions, for the four-MS-gate tests, these numbers are lower by about 5% (20%, 25% and 30%), since deeper circuits show higher contrast. On the downside, average fidelities of the four-MS-gate

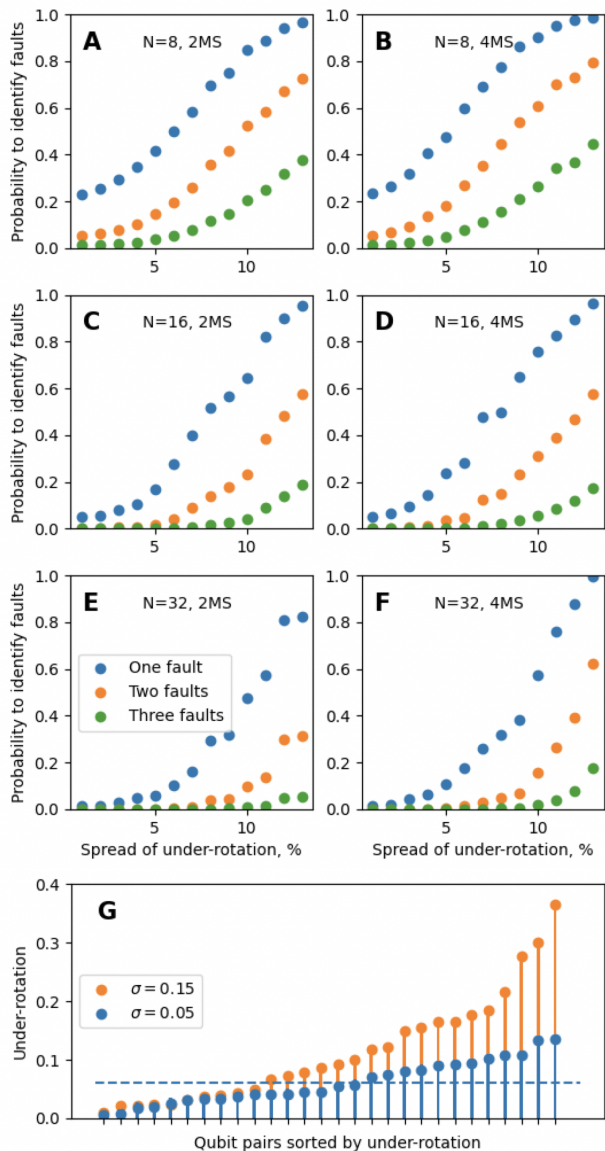


Figure 9: Simulated probabilities to identify one, two and three faulty gates (panels A-F) depending on the Gaussian spread of under-rotated gates in the presence of uniformly spread under-rotation up to 6% (dashed line on panel G) for 8, 16 and 32 qubits tested with two- and four-MS-gate tests. Two sorted generated distributions of gates by under-rotations are shown for $\sigma = 0.05$ and $\sigma = 0.15$ on panel G.

tests decay faster with the number of qubits in the presence of other noise sources.

Figure 8 shows that two faults that are too close in magnitude cannot be separated, which can scramble test syndromes. Table 2 gives estimates of the probability to correctly identify faulty gates

Table 2: Probabilities to identify faulty gates in the presence of one, two, and three faults on 8, 16, and 32 qubits.

n	Qubits	1 Fault	2 Faults	3 Faults
3	8	100%	47%	22%
4	16	100%	23%	5%
5	32	100%	12%	1%

for 8, 16, and 32 qubits, based on how the uniqueness of syndromes degenerates with the increased number of faults.

Using the results of Figure 8 and Table 2, we estimate success probabilities of identifying faulty couplings for under-rotation distributions similar to the experimentally observed distribution (Figure 7C). Focusing now on the spread of under-rotations identified in the previous section, Figure 9 shows the success probability to correctly identify the faulty coupling as a function of the % spread of the under-rotation. Considered are both two- and four-MS-gate tests, with larger number of qubits (8, 16, and 32).

The distribution of faults by under-rotations is assumed to be as follows. For up to 6% under-rotations, we use a uniformly random distribution. The choice of 6% is motivated by the calibration threshold that can be used in practice. For larger under-rotations, we use a right-tail Gaussian distribution centered at 6%, capturing the observed phenomenon of largely miscalibrated gates (orange points on Figure 7C). The under-rotations sampled from this composite distribution are shown on Figure 9 for $\sigma = 0.05$ and $\sigma = 0.15$.¹⁰ On average, as the spread increases, the errors are more separated by magnitude, the efficiency of detection increases not just for one but for multiple largest ones. The four-MS-gate tests show faster improvement due to higher contrast. Note the improvement is slightly dampened due to the larger effect of the 10% random amplitude noise on the four-MS-gate tests over their two-MS counterparts.

8 DISCUSSION

As ion-trap QCs scale up to attain quantum advantage, their all-pairs qubit couplings give a significant boost in computational power [23]. However, those qubit couplings require individual calibration and tend to gradually lose calibration. Their recalibration is already consuming a significant portion of the ion-trap QC lifecycle and will only grow as a fraction due to their $\binom{N}{2}$ scaling.

Our fault-detection strategy avoids costly recalibration of all couplings and in many cases may postpone recalibration since quantum circuits can be mapped around a small number of poorly calibrated qubit couplings. Compared to binary search, our combinatorial testing approach almost entirely avoids adaptive tests.

Consider how an adaptation-based test on an ion-trap QC is performed:

- Step 1 – A predetermined set of test circuits, each requiring qubit initialization, quantum gate execution, and qubit readouts, is run on a QC, repeated r times.

¹⁰Visually speaking, the composite distribution is flat up to 6% at a and then drops off according to the Gaussian distribution with the peak value of a . Normalization of the distribution function to one determines $a(\sigma) = 1/(0.06 + \sigma\sqrt{\pi/2})$.

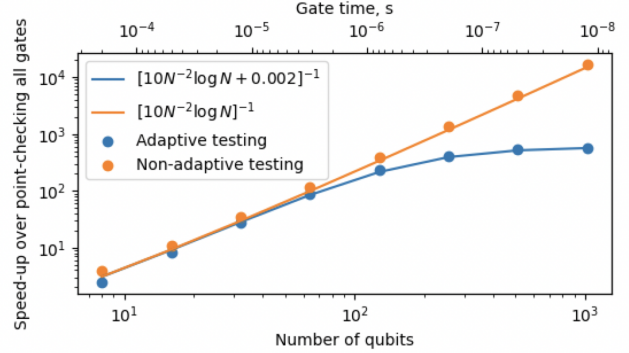


Figure 10: Speed-up for adaptive and non-adaptive testing compared to all-gate point-checks as a function of the number of qubits, N , assuming the gate time scales as $1/N^2$ starting with 0.2 ms for eight qubits. The speed-up for the adaptive testing plateaus due to the compilation time that depends on the number of couplings (blue line). It is still about 10^3 times smaller than the processing time required per point-check. The speed-up for the non-adaptive testing is projected to grow as $N^2/\log N$ (orange line).

- Step 2 – A conventional computer receives the readout results, determines the error syndrome that may involve measurement-error correction on the readouts, and identifies the next batch of tests to be run on an ion-trap QC.
- Step 3 – An ion-trap QC controller receives the next test instruction, compiles the control pulse according to the instruction, and uploads the compiled pulse.

The cost of adaptation can be estimated as the time taken by Steps 2 and 3, which may be significant compared to that of Step 1 (see Figure 10), especially in the regime where quantum operations become faster, an expected future for ion-trap QCs.

In some instances, quantum circuits to be run on an ion-trap QC do not require all qubit couplings to be used (Figure 11). In this case, an identified faulty qubit coupling can simply be avoided from being used, instead of executing the calibration process for the coupling. In fact, more than one faulty qubit couplings can be tolerated, as more become detected, as per Corollary 5.12, until an input quantum circuit to run can no longer be adequately mapped to an ion-trap QC to avoid all known faulty qubit couplings. A related work that aims to constructively determine the minimal set of qubit couplings that needs to be calibrated for a given batch of input quantum circuits is available in [22]. Our detection-based strategy offers a complementary solution to reducing the resource overhead for qubit coupling calibrations on ion-trap QCs.

9 CONCLUSIONS AND OUTLOOK

Ion-trap quantum computers are a fledgling technology with a multiyear track record of commercial cloud-based availability and significant upside potential. Key advantages include (1) chip-based technology with no need for exorbitant cooling equipment, (2) long qubit decoherence times T_1 and T_2 , (3) high-fidelity gates,



Figure 11: Number of utilized couplings (panel A) and their fraction of the total number of couplings (panel B) as a function of the number of qubits used in real-life quantum circuits [22]. The average number of utilized gates scales as $\sim 1/3$ of the total number of available gates (blue line).

and (4) the availability of all-pair qubit couplings. Near-term priorities include technology development, more accurate quantum control, and more effective lifecycle management. Our work improves the efficiency of periodic recalibration of qubit couplings by making them selective, based on an efficient fault-testing strategy. To enable this strategy, we developed a fault model for dominant faults. Our contributions are validated with formal proofs, physical experiments with commercial ion-trap quantum computers, and numerical simulations that show a good agreement with physical experiments and attractive scaling with the number of qubits.

The main impact of our work is in increasing the uptime of commercial QCs by reducing the fraction of their lifecycle dedicated to recalibration. Compared to today's strategy that would take over a minute for a full characterization of every coupling, our strategy, applied to an 11-qubit system [41] can diagnose the full system in ten seconds. While the number of qubits today is too small to fully illustrate the advantages of our diagnostic strategy, the advantage will grow more pronounced as ion-trap QCs scale. Future revisions of ion-trap platforms will improve basic technology (lasers, detectors) and quantum control (electric fields, beam alignment and power), as well as ion-trap capacity. Under such technology scaling, it will be particularly important to maintain all-pairs qubit connectivity — a major advantage of ion traps over solid-state quantum computing technologies that are limited to nearest-neighbor qubit couplings[21]. As the number of qubits grows, the number of qubit pairs grows faster, making old-style recalibration unsustainable. Our test-based recalibration facilitates more attractive scaling.

REFERENCES

- [1] C. J. Ballance, T. P. Harty, N. M. Linke, M. A. Sepiol, and D. M. Lucas. 2016. High-Fidelity Quantum Logic Gates Using Trapped-Ion Hyperfine Qubits. *Phys. Rev. Lett.* 117 (Aug 2016), 060504. Issue 6. <https://doi.org/10.1103/PhysRevLett.117.060504>
- [2] Reinhold Blümel, Nikodem Grzesiak, and Yunseong Nam. 2019. Power-optimal, stabilized entangling gate between trapped-ion qubits. arXiv:1905.09292 [quant-ph]
- [3] Reinhold Blümel, Nikodem Grzesiak, Nhung H. Nguyen, Alaina M. Green, Ming Li, Andrii Maksymov, Norbert M. Linke, and Yunseong Nam. 2021. Efficient Stabilized Two-Qubit Gates on a Trapped-Ion Quantum Computer. *Phys. Rev. Lett.* 126 (Jun 2021), 220503. Issue 22. <https://doi.org/10.1103/PhysRevLett.126.220503>
- [4] J.-S. Chen, K. Wright, N. C. Piseni, D. Murphy, K. M. Beck, K. Landsman, J. M. Amini, and Y. Nam. 2020. Efficient-sideband-cooling protocol for long trapped-ion chains. *Phys. Rev. A* 102 (Oct 2020), 043110. Issue 4. <https://doi.org/10.1103/PhysRevA.102.043110>
- [5] D. A. Church. 1969. Storage-Ring Ion Trap Derived from the Linear Quadrupole Radio-Frequency Mass Filter. *Journal of Applied Physics* 40, 8 (1969), 3127–3134. <https://doi.org/10.1063/1.1658153> arXiv:https://doi.org/10.1063/1.1658153
- [6] S. Crain, C. Cahall, G. Vrijsen, E. E. Wollman, M. D. Shaw, V. B. Verma, S. W. Nam, and J. Kim. 2019. High-Speed, Low-Crosstalk Detection of a Trapped $^{171}\text{Yb}^+$ Ion Ancilla Qubit using Superconducting Nanowire Single Photon Detectors. *Communications Physics* 2 (2019). <https://doi.org/10.1038/s42005-019-0195-8>
- [7] Joseph Emerson, Robert Alicki, and Karol Życzkowski. 2005. Scalable noise estimation with random unitary operators. *Journal of Optics B: Quantum and Semiclassical Optics* 7, 10 (sep 2005), S347–S352. <https://doi.org/10.1088/1464-4266/7/10/021>
- [8] Alexander Erhard, Joel J. Wallman, Lukas Postler, Michael Meth, Roman Stricker, Esteban A. Martinez, Philipp Schindler, Thomas Monz, Joseph Emerson, and Rainer Blatt. 2019. Characterizing large-scale quantum computers via cycle benchmarking. *Nature Communications* 10, 1 (Nov 2019), 1–7. <https://doi.org/10.1038/s41467-019-13068-7>
- [9] Edward Farhi, Jeffrey Goldstone, and Sam Gutmann. 2014. A Quantum Approximate Optimization Algorithm. arXiv:1411.4028 [quant-ph]
- [10] J. P. Gaebler, T. R. Tan, Y. Lin, Y. Wan, R. Bowler, A. C. Keith, S. Glancy, K. Coakley, E. Knill, D. Leibfried, and D. J. Wineland. 2016. High-Fidelity Universal Gate Set for $^9\text{Be}^+$ Ion Qubits. *Phys. Rev. Lett.* 117 (Aug 2016), 060505. Issue 6. <https://doi.org/10.1103/PhysRevLett.117.060505>
- [11] Todd J. Green and Michael J. Biercuk. 2015. Phase-Modulated Decoupling and Error Suppression in Qubit-Oscillator Systems. *Phys. Rev. Lett.* 114 (Mar 2015), 120502. Issue 12. <https://doi.org/10.1103/PhysRevLett.114.120502>
- [12] Nikodem Grzesiak, Reinhold Blümel, Kenneth Wright, Kristin M. Beck, Neal C. Piseni, Ming Li, Vandiver Chaplin, Jason M. Amini, Shantanu Debnath, Jwo-Sy Chen, and Yunseong Nam. 2020. Efficient arbitrary simultaneously entangling gates on a trapped-ion quantum computer. *Nature Communications* 11, 1 (Jun 2020), 1–6. <https://doi.org/10.1038/s41467-020-16790-9>
- [13] T. P. Harty, D. T. C. Allcock, C. J. Ballance, L. Guidoni, H. A. Janacek, N. M. Linke, D. N. Stacey, and D. M. Lucas. 2014. High-Fidelity Preparation, Gates, Memory, and Readout of a Trapped-Ion Quantum Bit. *Phys. Rev. Lett.* 113 (Nov 2014), 220501. Issue 22. <https://doi.org/10.1103/PhysRevLett.113.220501>
- [14] Honeywell. 2021. <https://www.honeywell.com/en-us/company/quantum> (Accessed May 20, 2021).
- [15] IBM. 2021. <https://www.ibm.com/quantum-computing/> (Accessed May 20, 2021).
- [16] Angus Kan and Yunseong Nam. 2021. Lattice Quantum Chromodynamics and Electrodynamics on a Universal Quantum Computer. *Submitted to PRX Quantum* (2021).
- [17] A. C. Lee, J. Smith, P. Richerme, B. Neyenhuis, P. W. Hess, J. Zhang, and C. Monroe. 2016. Engineering large Stark shifts for control of individual clock state qubits. *Phys. Rev. A* 94 (Oct 2016), 042308. Issue 4. <https://doi.org/10.1103/PhysRevA.94.042308>
- [18] Joonho Lee, Dominic W. Berry, Craig Gidney, William J. Huggins, Jarrod R. McClean, Nathan Wiebe, and Ryan Babbush. 2021. Even More Efficient Quantum Computations of Chemistry Through Tensor Hypercontraction. *PRX Quantum* 2 (Jul 2021), 030305. Issue 3. <https://doi.org/10.1103/PRXQuantum.2.030305>
- [19] Pak Hong Leung, Kevin A. Landsman, Caroline Figgatt, Norbert M. Linke, Christopher Monroe, and Kenneth R. Brown. 2018. Robust 2-Qubit Gates in a Linear Ion Crystal Using a Frequency-Modulated Driving Force. *Physical Review Letters* 120, 2 (Jan 2018), 020501. <https://doi.org/10.1103/physrevlett.120.020501>
- [20] Ming Li, Kenneth Wright, Neal C. Piseni, Kristin M. Beck, Jason H. V. Nguyen, and Yunseong Nam. 2020. Generalized Hamiltonian to describe imperfections in ion-light interaction. *Physical Review A* 102, 6 (Dec 2020), 062616. <https://doi.org/10.1103/physreva.102.062616>
- [21] Norbert M. Linke, Dmitri Maslov, Martin Roetteler, Shantanu Debnath, Caroline Figgatt, Kevin A. Landsman, Kenneth Wright, and Christopher Monroe. 2017. Experimental comparison of two quantum computing architectures. *Proceedings of the National Academy of Sciences* 114, 13 (Mar 2017), 3305–3310. <https://doi.org/10.1073/pnas.1618020114>

- [22] Andrii Maksymov, Pradeep Niroula, and Yunseong Nam. 2021. Optimal calibration of gates in trapped-ion quantum computers. *Quantum Science and Technology* 6, 3 (jun 2021), 034009. <https://doi.org/10.1088/2058-9565/abf718>
- [23] Dmitri Maslov. 2017. Basic circuit compilation techniques for an ion-trap quantum machine. *New Journal of Physics* 19, 2 (feb 2017), 023035. <https://doi.org/10.1088/1367-2630/aa5e47>
- [24] Dmitri Maslov, Yunseong Nam, and Jungsang Kim. 2019. An Outlook for Quantum Computing [Point of View]. *Proc. IEEE* 107, 1 (2019), 5–10. <https://doi.org/10.1109/JPROC.2018.2884353>
- [25] J. True Merrill and Kenneth R. Brown. 2012. Progress in compensating pulse sequences for quantum computation. arXiv:1203.6392 [quant-ph]
- [26] J. True Merrill, S. Charles Doret, Grahame Vittorini, J. P. Addison, and Kenneth R. Brown. 2014. Transformed composite sequences for improved qubit addressing. *Phys. Rev. A* 90 (Oct 2014), 040301. Issue 4. <https://doi.org/10.1103/PhysRevA.90.040301>
- [27] Yunseong Nam and Dmitri Maslov. 2019. Low-cost quantum circuits for classically intractable instances of the Hamiltonian dynamics simulation problem. *npj Quantum Information* 5, 1 (May 2019), 1–8. <https://doi.org/10.1038/s41534-019-0152-0>
- [28] Yunseong Nam, Neil J. Ross, Yuan Su, Andrew M. Childs, and Dmitri Maslov. 2018. Automated optimization of large quantum circuits with continuous parameters. *npj Quantum Information* 4, 1 (May 2018), 1–12. <https://doi.org/10.1038/s41534-018-0072-4>
- [29] Y. S. Nam and R. Blümel. 2015. Analytical formulas for the performance scaling of quantum processors with a large number of defective gates. *Phys. Rev. A* 92 (Oct 2015), 042301. Issue 4. <https://doi.org/10.1103/PhysRevA.92.042301>
- [30] Michael A. Nielsen and Isaac L. Chuang. 2011. *Quantum Computation and Quantum Information: 10th Anniversary Edition* (10th ed.). Cambridge University Press, USA.
- [31] Wolfgang Paul. 1990. Electromagnetic traps for charged and neutral particles. *Rev. Mod. Phys.* 62 (Jul 1990), 531–540. Issue 3. <https://doi.org/10.1103/RevModPhys.62.531>
- [32] Alberto Peruzzo, Jarrod McClean, Peter Shadbolt, Man-Hong Yung, Xiao-Qi Zhou, Peter J. Love, Alán Aspuru-Guzik, and Jeremy L. O’Brien. 2014. A variational eigenvalue solver on a photonic quantum processor. *Nature Communications* 5, 1 (Jul 2014), 1–7. <https://doi.org/10.1038/ncomms5213>
- [33] Rigetti. 2021. <https://www.rigetti.com> (Accessed May 20, 2021).
- [34] Alireza Seif, Kevin A. Landsman, Norbert M Linke, Caroline Figgatt, C Monroe, and Mohammad Hafezi. 2018. Machine learning assisted readout of trapped-ion qubits. *Journal of Physics B: Atomic, Molecular and Optical Physics* 51, 17 (Aug 2018), 174006. <https://doi.org/10.1088/1361-6455/aad62b>
- [35] C Shen and L-M Duan. 2012. Correcting detection errors in quantum state engineering through data processing. *New J. Phys.* 14, 5 (may 2012), 053053.
- [36] Yaoyun Shi. 2003. Both Toffoli and Controlled-NOT Need Little Help to Do Universal Quantum Computing. *Quantum Info. Comput.* 3, 1 (Jan. 2003), 84–92.
- [37] Peter W. Shor. 1997. Polynomial-Time Algorithms for Prime Factorization and Discrete Logarithms on a Quantum Computer. *SIAM J. Comput.* 26, 5 (Oct 1997), 1484–1509. <https://doi.org/10.1137/s0097539795293172>
- [38] Anders Sørensen and Klaus Mølmer. 1999. Quantum Computation with Ions in Thermal Motion. *Phys. Rev. Lett.* 82 (Mar 1999), 1971–1974. Issue 9. <https://doi.org/10.1103/PhysRevLett.82.1971>
- [39] Anders Sørensen and Klaus Mølmer. 2000. Entanglement and quantum computation with ions in thermal motion. *Phys. Rev. A* 62 (Jul 2000), 022311. Issue 2. <https://doi.org/10.1103/PhysRevA.62.022311>
- [40] Pengfei Wang, Chun-Yang Luan, Mu Qiao, Mark Um, Junhua Zhang, Ye Wang, Xiao Yuan, Mile Gu, Jingning Zhang, and Kihwan Kim. 2021. Single ion qubit with estimated coherence time exceeding one hour. *Nature Communications* 12, 1 (Jan 2021). <https://doi.org/10.1038/s41467-020-20330-w>
- [41] K. Wright, K. M. Beck, S. Debnath, J. M. Amini, Y. Nam, N. Grzesiak, J.-S. Chen, N. C. Panti, M. Chmielewski, C. Collins, K. M. Hudek, J. Mizrahi, J. D. Wong-Campos, S. Allen, J. Apisdorf, P. Solomon, M. Williams, A. M. Ducore, A. Blinov, S. M. Kreikebier, V. Chaplin, M. Keesan, C. Monroe, and J. Kim. 2019. Benchmarking an 11-qubit quantum computer. *Nature Communications* 10, 1 (Nov 2019), 1–6. <https://doi.org/10.1038/s41467-019-13534-2>
- [42] Yukai Wu, Sheng-Tao Wang, and L.-M. Duan. 2018. Noise analysis for high-fidelity quantum entangling gates in an anharmonic linear Paul trap. *Phys. Rev. A* 97 (Jun 2018), 062325. Issue 6. <https://doi.org/10.1103/PhysRevA.97.062325>
- [43] Shi-Liang Zhu, C. Monroe, and L.-M. Duan. 2006. Trapped Ion Quantum Computation with Transverse Phonon Modes. *Physical Review Letters* 97, 5 (Aug 2006), 050505. <https://doi.org/10.1103/physrevlett.97.050505>